# The effect of facets reflectivity on the static characteristics of (DFB) semiconductor laser

**Conference Paper** · October 2018

DOI: 10.1109/CISTEM.2018.8613390



**2 authors:**

Mohammed Mehdi Bouchene
Université 8 mai 1945 - Guelma
**11** PUBLICATIONS **17** CITATIONS
SEE PROFILE

Rachid Hamdi
Université 8 mai 1945 - Guelma
**46** PUBLICATIONS **89** CITATIONS
SEE PROFILE

# The effect of facets reflectivity on the static characteristics of (DFB) semiconductor laser

Mohammed Mehdi Bouchene
Laboratoire des Télécommunications (LT)
Université 8 mai 1945 Guelma
Guelma, Algeria
E-mail:bouchene.mehdi@univ-guelma.dz

Rachid Hamdi
Laboratoire des Télécommunications (LT)
Université 8 mai 1945 Guelma
Guelma, Algeria
E-mail : hamdi.rachid@univ-guelma.dz

*Abstract*— **In this paper, we present a rigorous approach based on split-step time-domain dynamic modeling (SS-TDM) algorithm using to solve the time-dependent coupled wave equations of the time-domain traveling-wave (TDTW) model to investigate the effect of facets reflectivity on the Light-Current characteristics of (DFB) semiconductor laser for different values the coupling coefficient. The simulation results show that using high reflection coating on the front facet and low reflection coating on the back facet with a proper diffraction grating can significantly improve the power-conversion efficiency of the (DFB) semiconductor laser.**

***Keywords— DFB laser, Power conversion efficiency, Time-domain modeling.***

## I. INTRODUCTION

Distributed feedback semiconductor (DFB) lasers are largely exploited in high-speed long-distance fiber-optic communication systems due to their attractive properties such as wavelength stability and narrow spectral width [1]. In the last three decades, an enormous effort has been devoted to optimize the power conversion efficiency of semiconductor lasers [2-4]. For DFB lasers the most useful techniques to enhance the power conversion efficiency while maintaining high side mode suppression ratio (SMSR) and narrow spectral width are: second-order grating [5], and complex-coupled (DFB) lasers [6].

For numerical simulation, two main approaches have been used to determine the static characteristics of semiconductor lasers: steady-state analysis, and large signal analysis by solving the rate equations model [7]. For steady-state analysis, Light-current characteristics of the laser are obtained by solving the rate equations model under static condition, then obtain an analytical expression for the threshold current and the slope efficiency. However, this is valid only for the Fabry-Pérot lasers where the feedback mechanism is originated from the end facets. Unlike (F-P) lasers, the feedback mechanism in (DFB) lasers is distributed throughout the laser cavity due to grating, and it have been shown recently that even the shape of the grating and phase-shift position have an effect on the lasing threshold current and slope efficiency on multiple-phase-shift DFB laser with distributed coupling coefficient [8]. Indeed, these methods provide simplicity with broad application to different types of edge-emitting semiconductor lasers. However, both of these approaches ignore crucial elements for a proper analysis of (DFB) lasers such as the diffraction grating and the non-uniform distribution of the photon and carrier density which they have a major importance in (DFB) lasers modeling. Yet, none of these methods take into account the facets phase in their formalism; therefore, a coupled-wave approach is required for this kind of lasers [9].

The purpose of the present paper is to study the impact of the end facets reflectivity on the lasing threshold current and the slope efficiency of (DFB) semiconductor laser for different values the coupling coefficient by using a unified model such as the time-domain traveling-wave (TDTW) model and solve the time-dependent coupled wave equations of this model by using an efficient algorithm such as the split-step time-domain modeling (SS-TDM) algorithm.

The paper is organized as follows. In the next section, we describe briefly the time-domain traveling-wave (TDTW) model and the split-step time-domain dynamic modeling (SS-TDM) algorithm. We then present the simulation results of the static characteristics of (DFB) laser and interpret them physically. Finally, conclusion and perspectives are presented in last section.

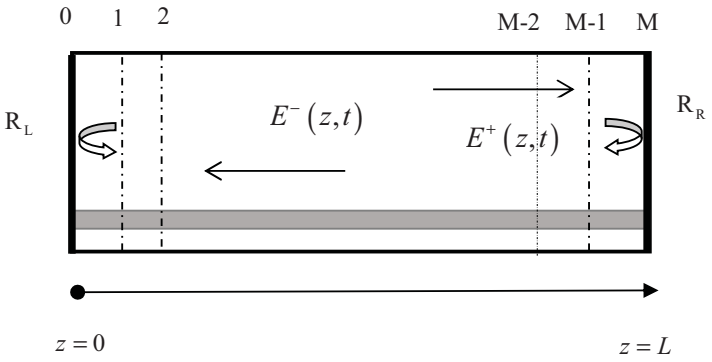


Fig. 1. Basic schematic representation of Laser cavity with M sections

## II. NUMERICAL METHOD

The total optical field inside the (DFB) laser cavity can be expressed as a combination of counter-propagating travelling waves as shown in fig.1, defined as follows:

$$E(z,t) = \left[E(z,t)\right]\exp(j\omega_0 t) = \left[E^+(z,t)\exp(-j\beta_0 z) + E^-(z,t)\exp(j\beta_0 z)\right]\exp(j\omega_0 t) \quad (1)$$

$E^+$ and $E^-$ are respectively the forward and backward slowly varying amplitude of the traveling optical field, $\beta_0$ is

978-1-5386-4988-6/18/$31.00 ©2018 IEEE

Bragg propagation constant, and $\omega_0$ is the reference angular frequency near to lasing operation.

The time-dependent coupled-wave equations for forward and backward optical fields called an advection wave equation, is used to describe the time and spatial development of the field inside the laser cavity, for both forward and backward waves, we have [10]:

$$\frac{1}{C_g}\frac{\partial E^+}{\partial t}+\frac{\partial E^+}{\partial z}=(G-\mathrm{j}\delta)E^+ + j\kappa E^- + \xi_+ \tag{2}$$

$$\frac{1}{C_g}\frac{\partial E^-}{\partial t}-\frac{\partial E^-}{\partial z}=(G-\mathrm{j}\delta)E^- + j\kappa E^+ + \xi_- \tag{3}$$

$C_g$ is the group velocity, $\kappa$ is the coupling coefficient. $G$ is the net optical gain and it is given by:

$$G=\frac{\Gamma G_N\{N-N_0\}}{2(1+\varepsilon S)}-\frac{\alpha_m}{2} \tag{4}$$

$S$ is the photon density and it is given by:

$$S(z,t)=\left|E^+(z,t)\right|^2+\left|E^-(z,t)\right|^2 \tag{5}$$

$\alpha_m$ is the material loss, $\Gamma$ is the optical mode confinement factor, $\delta$ is the detuning factor defined as:

$$\delta(z,t)=\frac{2\pi}{\lambda_0}n_{eff}(z,t)-\frac{\pi}{\Lambda} \tag{6}$$

$n_{eff}$ is the effective refractive index, which is given by:

$$n_{eff}(z,t)=n_{eff}{}^0-\Gamma\alpha_m\left(\frac{\Gamma G_N\{N(z,t)-N_0\}}{2(1+\varepsilon S(z,t))}\right)\frac{\lambda_0}{4\pi} \tag{7}$$

$\xi_+(z,t)$ and $\xi_-(z,t)$ are the spontaneous emission noises associated with the forward and backward traveling waves which can be approximated as a Gaussian random processes that have a zero mean : $\langle\xi(z,\mathrm{t}),\xi(z,\mathrm{t})\rangle=0$, and their correlation function is defined as follows:

$$\left\langle\xi(z,\mathrm{t}),\xi^*(z`,\mathrm{t}`)\right\rangle=K\Gamma_{sp}\beta R_{sp}L\delta(t-t`)\delta(z-z`)/C_g{}^2 \tag{8}$$

$K$ is Peterman coefficient, $\Gamma_{sp}$ is the confinement factor of spontaneous emission, $R_{sp}$ is the rate of spontaneous emission, and $L$ is the laser cavity length.

The boundary conditions are defined at rear and the front facets of the laser as follows (fig. 1) [11]:

$$E^+((z=0),t)=\sqrt{R_L}\exp(j\varphi_L)E^-(z=0,t) \tag{9}$$

$$E^-(z=L,t)=\sqrt{R_R}\exp(j\varphi_R)E^-(z=L,t) \tag{10}$$

$R_L$, $R_R$ are the left and the right facets power reflectivity, while $\varphi_L$, $\varphi_R$ are left and the right facets phase. In our modeling, we ignore the effect of random facet phase on the lasing characteristics.

The rate equation for carrier density is given by [5]:

$$\frac{\partial N(t,z)}{\partial t}=\frac{J(t,z)}{ed}-AN-BN^2-CN^3-GC_GS \tag{11}$$

The output power from the left and right facets respectively is given by [12] :

$$P_L(t)=\frac{dw}{\Gamma}C_g\frac{hc}{\lambda}(1-R_L)\left(\left|E^+(0,t)\right|^2+E^-\left|(0,t)\right|^2\right) \tag{12}$$

$$P_R(t)=\frac{dw}{\Gamma}C_g\frac{hc}{\lambda}(1-R_R)\left(\left|E^+(L,t)\right|^2+E^-\left|(L,t)\right|^2\right) \tag{13}$$

$d$ and $w$ are respectively the active layer width and thickness, $h$ is Planck constant, $c$ is the speed of light.

To solve the time-dependent coupled-wave equations in (2), (3), the laser cavity is divided into a finite number of sections $M$ with equal length $\Delta z$, as shown in fig. 1 such as:

$$\Delta z=\frac{M}{L} \tag{14}$$

The final scheme of the (SS-TDM) algorithm is divided into two steps, can be written as follows [13,14]:

First step:

$$\begin{bmatrix}E^+(z+\Delta z,t)\\E^-(z,t)\end{bmatrix}=\begin{bmatrix}\exp\{(\mathrm{G}-\mathrm{i}\delta)\Delta z\} & 0\\0 & \exp\{(\mathrm{G}-\mathrm{i}\delta)\Delta z\}\end{bmatrix}\begin{bmatrix}E^+(z,t-\Delta t)\\E^-(z+\Delta z,t-\Delta t)\end{bmatrix}+\Delta z\begin{bmatrix}\xi_+(z,t)\\\xi_-(z,t)\end{bmatrix} \tag{15}$$

Second step:

$$\begin{bmatrix}E^+(z+\Delta z,t)\\E^-(z,t)\end{bmatrix}=\begin{bmatrix}\sec h(\kappa_( z) & j\tanh(\kappa z)\\j\tanh(\kappa z) & \sec h(\kappa z)\end{bmatrix}\begin{bmatrix}E^+(z,t)\\E^-(z+\Delta z,t)\end{bmatrix} \tag{16}$$

$\Delta t$ is the simulation time step, and it related to the section length $\Delta z$ by:

$$\Delta z=C_g\Delta t \tag{17}$$

This relation represents the stability condition of the (SS-TDM) algorithm. However, the spatial step size $\Delta z$ have a direct impact on the CPU time. Thus, the larger the number of sections is, the longer the required simulation time eventually be. For the (SS-TDM) algorithm a number of sections equal to $\mathrm{M}=40$ gives reasonable adjustment between calculation accuracy and time.

The rate equation of the carrier density is converted also to difference equation by using first-order approximation of derivatives by finite differences which results in:

$$N(z,t+\Delta t)=N+\Delta t\left(\frac{J}{ed}-AN-BN^2-CN^3-GC_GS\right) \tag{18}$$

For numerical implementation, we first define laser material and structure parameters. The optical fields $E^+$ and $E^-$ are computed with initial spontaneous emission noise terms which are updated at each grid point at the next time step by (15), (16) using the old fields computed at previous time step as an input, carrier density $N$ at each section is simultaneously calculated by (18). When the optical fields arrive at the end facets, the boundary conditions defined in

(9), (10) must be satisfied. These steps are repeated until the simulation stop time is reached.

TABLE I. PARAMETERS USED IN THE SIMULATION

| Parameter | Value | Description | Unit |
|---|---|---|---|
| $A$ | 1 | Linear recombination coefficient | $10^{10}$ s$^{-1}$ |
| $B$ | 1 | Bimolecular coefficient | $10^{-10}$ cm$^{3/s}$ |
| $C$ | 7 | Auger coefficient | $10^{-29}$cm$^{6/s}$ |
| $G_N$ | 2.5 | Differential field-gain | $10^{-16}$cm$^2$ |
| $\alpha_m$ | 10 | Waveguide loss | cm$^{-1}$ |
| $N_0$ | 1 | Transparency carrier density | $10^{18}$cm$^3$ |
| $n_{eff\,0}$ | 3.2 | Effective phase refractive index | |
| $n_g$ | 3.6 | Effective group refractive index | |
| $L$ | 600 | Laser cavity length | µm |
| $\Lambda$ | 242.18 | Grating period | Nm |
| $w$ | 1.5 | Active layer width | µm |
| $d$ | 0.2 | Active layer thickness | µm |
| $\Gamma$ | 0.3 | Confinement factor | |
| $\lambda$ | 1550 | Wavelength lasing | nm |
| $\alpha_H$ | 4 | Linewidth enhancement factor | |
| $\varepsilon$ | 5 | Gain compression factor | $10^{-17}$cm$^3$ |
| $\beta$ | 5 $10^{-5}$ | Spontaneous emission coefficient | |
| $K$ | 1 | Peterman coefficient | |
| $\kappa$ | 30, 60, 80 | Coupling coefficient | cm$^{-1}$ |
| $J(t,z)$ | Variable | Current injection | mA |

## III. SIMULATION RESULTS AND DISCUSSIO

Based on the (SS-TDM) algorithm presented in the previous section, we simulate the static behavior of multi-quantum-well (MQW) uniform index-coupled DFB semiconductor laser with different values of facets reflectivity and coupling coefficient, the device parameters are listed in Table I. The static characteristics of the laser are obtained from the large-signal transient response illustrated in fig. 2 by biasing the laser at a given drive current then wait until the device reach the steady-state condition, then calculating the average output power to reduce impacts of the randomness nature of the spontaneous emission noise [8,15]. The laser output is considered on the right facet. The total simulation time is set 15 ns and the drive current step is 0.05 mA that ensure the establishment of steady state for low drive current. The output power is averaged over last 2 ns of the simulation time.

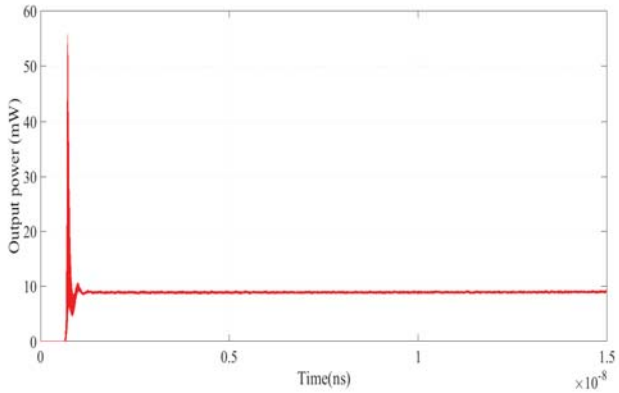


Fig. 2. Large-signal transient response of (DFB) laser for drive current 50 mA and antireflection (AR) coating on both facets

Fig. 3 shows the optical output power in (mW) versus the injection current in (mA) of a (DFB) laser with coupling coefficient equal to 30 cm$^{-1}$ ( $\kappa L = 1.8$ )for three end facets reflectivity configuration: For high reflectivity on the back facet with power reflectivity equal to 0.97 and low reflectivity on the front facet with power reflectivity equal to 0.1, and for low reflectivity on both facets with power reflectivity equal to 0.1, and for medium reflectivity on both facets with power reflectivity equal to 0.32. It can be seen that the lasing threshold current for the three end facets configuration is respectively: 9.94 mA, 13.95 mA and 10.6 mA, and the slope efficiency is respectively: 0.518 W/A, 0.306 W/A, 0.274 W/A. The slope efficiency is estimated by using linear least squares approximation after the stimulated emission become dominant.

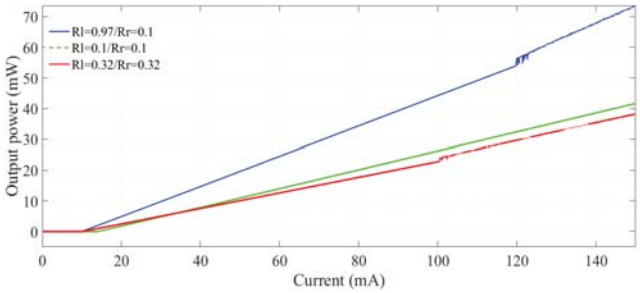


Fig. 3. Light-current curve of (DFB) laser for kappa 30 cm$^{-1}$. With different values of end facets reflectivity: (blue) $R_L$=0.97and $R_R$=0.1, (green) $R_L$=0.97 and $R_R$=0.1, (red) $R_L$=0.32 and $R_R$=0.32

This example shows clearly that by using a high reflectivity coating on back facet and low reflectivity coating on the front facet can reduce the lasing threshold current and increase significantly the slope efficiency. We notice also that medium reflectivity end facets configuration may have lower threshold current than the low reflectivity end facets configuration but this last has better slope efficiency, this is due to fact that the attenuation caused by the mirrors at the end facets is more prominent as the output power increases.

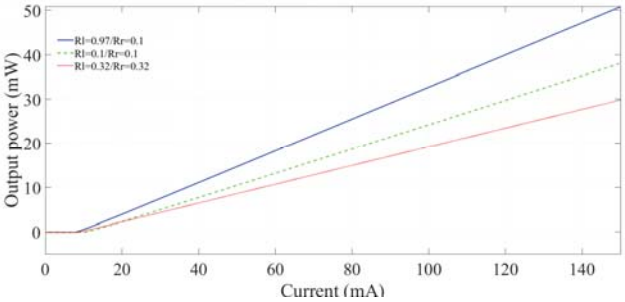


Fig. 4. Light-current curve of (DFB) laser for kappa 60 $cm^{-1}$. With different values of end facets reflectivity (blue) $R_L$=0.97and $R_R$=0.1, (green) $R_L$=0.97 and $R_R$=0.1, (red) $R_L$=0.32 and $R_R$=0.32

Fig. 2 illustrates Light-current characteristics of (DFB) laser for coupling coefficient equal to 60 $cm^{-1}$ ( $\kappa L = 3.6$ ), it can be seen that the threshold current for the three end facets configuration is respectively: 8.15 mA, 10.6 mA, 9.15 mA, and the slope efficiency is respectively : 0.187 W/A, 0.275 W/A, 0.212 W/A.

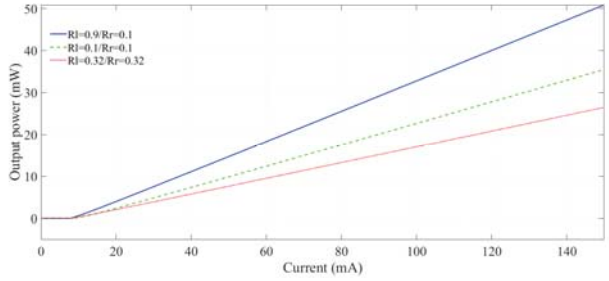


Fig. 5. Light-current curve of (DFB) laser for kappa 80 $cm^{-1}$. With different values of end facets reflectivity (blue) $R_L$=0.97and $R_R$=0.1, (green) $R_L$=0.97 and $R_R$=0.1, (red) $R_L$=0.32 and $R_R$=0.32

Fig.3 shows Light-current characteristics of (DFB) laser with coupling coefficient equal to 80 $cm^{-1}$ ( $\kappa L = 4.8$ ) for the three end facets configuration, it can be seen that the threshold current for the three end facets configuration is respectively: 8.1 mA, 9.35 mA, 8.7 mA and the slope efficiency is respectively : 0.36W/A, 0.254W/A, 0.187 W/A. Just by comparing the results obtained with different values of coupling coefficient, we conclude that the (DFB)laser has the best performance in terms of power conversion efficiency for configuration with high reflectivity coating on back facet and low reflectivity on the front facet and the static parameters threshold current and slope efficiency depend on coupling coefficient.

These results demonstrate that the diffraction grating and the grating shape have impact on the threshold current and the slope efficiency of the laser depending on end facets power reflectivity. Although, steady-state analysis or rate equations model does not take into account the coupling coefficient in their formalism, which could lead to inaccurate results in the analysis of the static characteristics of the (DFB) laser. On the other hand, the main disadvantage of the presented method is the huge computation time required because of the dynamical nature of the (SS-TDM) algorithm.

## IV. CONCLUSION

We have presented a rigorous method based on (SS-TDM) algorithm which help to simulate accurately the static characteristics of (DFB) laser. The proposed method can be applied any kind of (DFB) laser structure. The simulation results are obtained for a uniform index-coupled (DFB) laser operation around 1.55µm used in optical communication systems with different of facets reflectivity configuration for different values of coupling coefficient. The simulation results show that by optimizing the facets reflectivity and the grating shape, we can reduce the threshold current and increase the slope efficiency of the laser. Future work will aim to use the same approach to study the influence of random facets phase on the static characteristics of (DFB) laser.

## REFERENCES

[1] G. P.Agrawal, Fiber-Optic Communication Systems (Wiley, 2010).

[2] M. Beck, D. Hofstetter, T. Aellen, J. Faist, U. Oesterle, M. Ilegems,E. Gini, and H. Melchior, "Continuous wave operation of a mid-infrared semiconductor laser at room temperature," Science, vol. 295, pp. 301–305, 2002.

[3] K. Mukai, Y. Nakata, H. Shoji, S. Sugawara, K. Ohtsubo, N. Yokoyama,H. Ishikawa, "Lasing with low-threshold current and high-output power from columnar-shaped InAs/GaAs quantum dots," Electron. Lett., vol 34, pp. 1588–1590, 1998.

[4] H. Soda, Y. Kotaki, H. Sudo, H. Ishikawa, S. Yamakoshi, and H. Imai, "Stability in single longitudinal mode operation in GaInAsP/InP phase-adjusted DFB lasers," IEEE J. Quantum Electron., vol. 23, pp. 804-814, 1987.

[5] L. M. Zhang. S. F. Yu. M. C. Nowell. D. D. Marcenac. J. E. Carroll.and R. G. s'. Plumb, "Dynamic analysis of radiation and side-mode suppression in a second-order DFB laser using time domain large signal travelling wave model," IEEE J. Quantum Electron., vol. 30, pp.1389-1395, 1994.

[6] Z. M. Chuang, C. Y. Wang, W. Lin, H. H. Liao, J. Y. Su, and Y. K. Tu, "Very-low-threshold, high efficient, and low-chirp 1.55-µm complex-coupledDFB lasers with a current-blocking Grating,"IEEE Photon. Technol.Lett., vol. 8, no. 11, pp. 1438–1441, Nov. 1996

[7] K. Petermann, "Laser Diode Modulation and Noise, " Dordrecht, Netherlands:Kluwer, 1991

[8] M.M.Bouchene, R.Hamdi, "Effects of structural parameters on the Light-Current characteristics of multiple-phase-shift DFB semiconductor laser with distributed coupling coefficient," in Proc.second International Conference OPAL2018 (Optics and Photonics Algeria), USTO 5 – 7 May 2018, Oran, Algeria.

[9] Bouchene Mohammed Mehdi and Hamdi Rachid, "Study of Fabry-Pérot laser oscillation field spectrum using Traveling Wave Model" 3rd International Conference on Embedded Systems in Telecommunications and Instrumentation (ICESTI'16), October 24 – 26, 2016, Annaba, Algeria

[10] J.Carroll, J.Whiteaway, and D.Plumb "Distributed Feedback Semiconductor Lasers," IEE, 1998.

[11] Bouchene Mohammed Mehdi, "Comparison between rate equations model and traveling wave model in large signal transient response of FabryPérot Laser diodes," CiiT international journal of Digital Signal Processing, Vol 9, No 8 2017.

[12] H. Ghafouri-Shiraz, "Distributed Feedback Laser Diodes and OpticalTunable Filters, " New York: Wiley, 2003.

[13] B. Kim, Y. Chung, and J.-S. Lee, "An efficient split-step time-domain dynamic modeling of DFB/DBR laser diodes," IEEE J. Quantum Electron., vol. 36, pp. 787–794, July 2000.

[14] YANPING XI.: "One-Dimensional Simulation Methods for Distributed Feedback Semiconductor Lasers," PhD dissertation, University of Mcmaster, 2009.

[15] M.M.Bouchene, R.Hamdi, Q.Zou, "Theorical analysis of a monolithic all-active three-section semiconductor laser", Photonics Letters of Poland, Vol 9, No 4 2017